

Catalysis of H₂/D₂ Scrambling and Other H/D Exchange Processes by [Fe]-Hydrogenase Model Complexes

Xuan Zhao, Irene P. Georgakaki, Matthew L. Miller, Rosario Mejia-Rodriguez, Chao-Yi Chiang, and Marcetta Y. Darensbourg*

Department of Chemistry, Texas A&M University, College Station, Texas 77843

Received March 28, 2002

Protonation of the [Fe]-hydrogenase model complex (μ -pdt)[Fe(CO)₂(PMe₃)₂] (pdt = SCH₂CH₂CH₂S) produces a species with a high field ¹H NMR resonance, isolated as the stable {(μ -H)(μ -pdt)[Fe(CO)₂(PMe₃)₂]⁺[PF₆]⁻ salt. Structural characterization found little difference in the 2Fe2S butterfly cores, with Fe...Fe distances of 2.555(2) and 2.578(1) Å for the Fe–Fe bonded neutral species and the bridging hydride species, respectively (Zhao, X.; Georgakaki, I. P.; Miller, M. L.; Yarbrough, J. C.; Darensbourg, M. Y. *J. Am. Chem. Soc.* **2001**, *123*, 9710). Both are similar to the average Fe...Fe distance found in structures of three Fe-only hydrogenase active site 2Fe2S clusters: 2.6 Å. A series of similar complexes (μ -edt)-, (μ -o-xyldt)-, and (μ -SEt)[Fe(CO)₂(PMe₃)₂] (edt = SCH₂CH₂S; o-xyldt = SCH₂C₆H₄CH₂S), (μ -pdt)[Fe(CO)₂(PMe₂Ph)]₂, and their protonated derivatives likewise show uniformity in the Fe–Fe bond lengths of the neutral complexes and Fe...Fe distances in the cationic bridging hydrides. The positions of the PMe₃ and PMe₂Ph ligands are dictated by the orientation of the S–C bonds in the (μ -SRS) or (μ -SR)₂ bridges and the subsequent steric hindrance of R. The Fe^{II}(μ -H)Fe^{II} complexes were compared for their ability to facilitate H/D exchange reactions, as have been used as assays of H₂ase activity. In a reaction that is promoted by light but inhibited by CO, the {(μ -H)(μ -pdt)[Fe(CO)₂(PMe₃)₂]⁺ complex shows H/D exchange activity with D₂, producing {(μ -D)(μ -pdt)[Fe(CO)₂(PMe₃)₂]⁺ in CH₂Cl₂ and in acetone, but not in CH₃CN. In the presence of light, H/D scrambling between D₂O and H₂ is also promoted by the Fe^{II}(μ -H)Fe^{II} catalyst. The requirement of an open site suggests that the key step in the reactions involves D₂ or H₂ binding to Fe^{II} followed by deprotonation by the internal hydride base, or by external water. As indicated by similar catalytic efficiencies of members of the series, the nature of the bridging thiolates has little influence on the reactions. Comparison to [Fe]H₂ase enzyme active site redox levels suggests that at least one Fe^{II} must be available for H₂ uptake while a reduced or an electron-rich Fe^IFe^I metal–metal bonded redox level is required for proton uptake.

Introduction

The simplicity of the binuclear active site of [Fe]-H₂ase, Figure 1a,^{1–3} the limited involvement of protein residues in its first coordination sphere construction, and the distinct possibility that the site emerged billions of years ago and evolved in a preoxidizing terrestrial environment has inspired synthetic chemists to pursue organoiron model complexes as potential catalysts of H₂ production or uptake. Disulfidodironhexacarbonyl, (μ -S₂)Fe₂(CO)₆, a compound that could

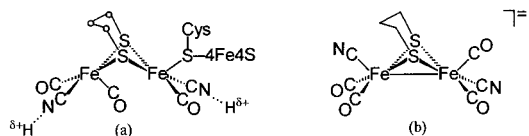


Figure 1. (a) Two-iron unit of the H-cluster, active site of Fe-hydrogenase.^{1–3} (b) Structure of (μ -SCH₂CH₂CH₂S)Fe₂(CO)₄(CN)₂²⁻.⁹

reasonably represent the mobilization of iron sulfide mineral by carbon monoxide in the genesis of a primordial catalyst,⁴ serves as synthetic entry into low valent dinuclear iron complexes. We and others have shown that transformation of it into a dithiolate bridged Fe^IFe^I complex is easy to accomplish,^{5–8} as is the subsequent displacement of two CO ligands by better donor ligands such as cyanide,^{6–10} Figure

(4) Cody, G. D.; Boctor, N. Z.; Filley, T. R.; Hazen, R. M.; Scott, J. H.; Sharma, A.; Yoder, H. S., Jr. *Science* **2000**, *289*, 1337.

* To whom correspondence should be addressed. E-mail: marcetta@mail.chem.tamu.edu.

(1) Peters, J. W.; Lanzilotta, W. N.; Lemon, B. J.; Seefeldt, L. C. *Science* **1998**, *282*, 1853.

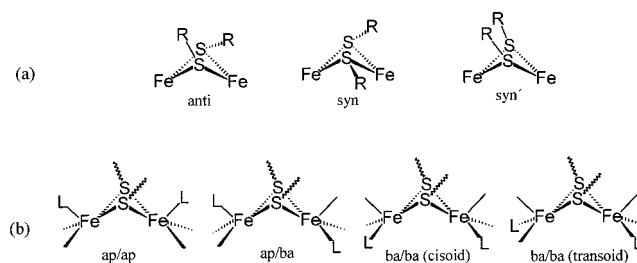
(2) Nicolet, Y.; Piras, C.; Legrand, P.; Hatchikian, C. E.; Fontecilla-Camps, J. C. *Structure* **1999**, *7*, 13.

(3) Nicolet, Y.; De Lacey, A. L.; Vernéde, X.; Fernandez, V. M.; Hatchikian, E. C.; Fontecilla-Camps, J. C. *J. Am. Chem. Soc.* **2001**, *123*, 1596.

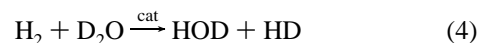
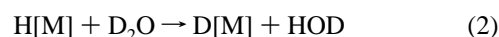
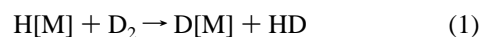
1b,⁹ or by phosphine.¹¹ Not only do the dicyano derivatives provide a formulation highly similar to that of the active site but also their central $[(\mu\text{-SRS})\text{Fe}_2]$ cores are structurally identical. Nevertheless, the enzyme has stabilized the active site structure in such a conformation that is more similar to the transition state of FeL_3 unit rotation rather than to the ground-state structure of the model complexes.¹² The metal–metal bonds of the cyanide- or phosphine-substituted binuclear complexes are sufficiently electron-rich to serve as bases toward protons, leading to binuclear oxidative addition and the formation of bridging hydride complexes, $[\text{Fe}^{\text{II}}(\mu\text{-H})\text{Fe}^{\text{II}}]^+$.^{13,14} The significance of this chemical access to the Fe^{II} oxidation state makes it possible for H_2 to bind, consistent with known $\eta^2\text{-H}_2$ in d^6 Fe^{II} complexes.¹⁵

The oxidation states of iron in the binuclear active site of $[\text{Fe}]\text{-H}_2\text{ase}$ have not been unambiguously established. The $\nu(\text{CO})$ and $\nu(\text{CN})$ stretching frequencies in FT-IR spectra of various redox levels of the enzyme are compatible with a range of oxidation states including $\text{Fe}^{\text{II}}\text{Fe}^{\text{II}}$, $\text{Fe}^{\text{II}}\text{Fe}^{\text{I}}$, and $\text{Fe}^{\text{I}}\text{Fe}^{\text{I}}$.^{3,16} Such redox states are not inconsistent with Mössbauer spectral results.¹⁷ Hence, the organometallic $[\text{Fe}^{\text{II}}\text{Fe}^{\text{II}}]$ and $[\text{Fe}^{\text{II}}(\mu\text{-H})\text{Fe}^{\text{II}}]^+$ complexes have been explored as functional models for H_2 binding, and activation.¹⁸ The latter model studies have used H/D exchange reactivity, similarly to assays used for enzyme activity, according to eqs 1–4.^{19–23} In addition to H/D scrambling in H_2/D_2 mixtures, and HD production in the $\text{H}_2/\text{D}_2\text{O}$ mixtures, the incorporation of deuterium into the bridging hydride complexes, represented by $\text{D}[\text{M}]$ in eqs 1 and 2, is also indicative of the heterolytic

Chart 1



activation of dihydrogen or dideuterium. It should be noted that, as of now, definitive proof of a metal hydride in biology is missing; however, such functional model studies as these provide a “smoking gun” for their presence.



The presence of substituent ligands with donor ability better than CO is crucial to the binuclear oxidative addition of H^+ to yield the $[\text{Fe}^{\text{II}}(\mu\text{-H})\text{Fe}^{\text{II}}]^+$ complexes from $(\mu\text{-SR})_2\text{-}[\text{Fe}(\text{CO})_2\text{L}]_2$. While PMe_3 is not as good a donor as is CN^- toward Fe^{I} , it is sufficiently stabilizing of Fe^{II} to permit the isolation of $\{(\mu\text{-H})(\mu\text{-pdt})[\text{Fe}(\text{CO})_2(\text{PMe}_3)_2]_2\}^+$, complex **3-H**⁺ ($\text{pdt} = \text{SCH}_2\text{CH}_2\text{CH}_2\text{S}$), without the complications of cyanide nitrogen protonation competing with protonation of the iron–iron bond.²⁴ Complex **3-H**⁺ was found to undergo H/D exchange in the presence of D_2 under photolysis to produce **3-D**⁺, as well as to catalyze the formation of HD in H_2/D_2 mixtures.¹⁸ These preliminary results led to the broader study described later of a series of $(\mu\text{-SRS})[\text{Fe}(\text{CO})_2(\text{PR}'_3)]_2$ and their conjugate acids, for factors which might affect their ability to serve as H/D exchange assay models of hydrogene-nase active sites.

Binuclear complexes of formulation $(\mu\text{-SR})_2[\text{Fe}(\text{CO})_2\text{L}]_2$, and the isomeric possibilities resulting from SR^- and L orientations, are well-known. In 1973, Ellgen and Gerlach interpreted kinetic parameters of CO/PR'_3 substitution according to the steric requirements of both SR and PR'_3 .²⁵ Even in the absence of X-ray crystal structures, their insight helped formulate the possibilities for structural isomers which derive from (a) positioning of the carbons α to the bridging sulfurs, in syn, syn', and anti conformations,²⁶ as well as (b) placing the phosphines in positions trans or cis to the metal–metal bond or bridging hydride, see Chart 1. Because the iron atoms of the neutral species are in pseudo-square-pyramidal coordination geometries, the positions of the

- (5) Seyferth, D.; Womack, G. B.; Gallagher, M. K.; Cowie, M.; Hames, B. W.; Fackler, J. P., Jr.; Mazany, A. M. *Organometallics* **1987**, *6*, 283.
- (6) Lawrence, J. D.; Li, H.; Rauchfuss, T. B.; Bénard, M.; Rohmer, M.-M. *Angew. Chem., Int. Ed.* **2001**, *40*, 1768.
- (7) Lyon, E. J.; Georgakaki, I. P.; Reibenspies, J. H.; Darensbourg, M. Y. *Angew. Chem., Int. Ed.* **1999**, *38*, 3178.
- (8) Le Cloirec, A.; Best, S. P.; Borg, S.; Davies, S. C.; Evans, D. J.; Hughes, D. L.; Pickett, C. J. *Chem. Commun.* **1999**, 2285.
- (9) Schmidt, M.; Contakes, S. M.; Rauchfuss, T. B. *J. Am. Chem. Soc.* **1999**, *121*, 9736.
- (10) Razavet, M.; Davies, S. C.; Hughes, D. L.; Pickett, C. J. *Chem. Commun.* **2001**, 847.
- (11) De Beer, J. A.; Haines, R. J. *J. Organomet. Chem.* **1972**, *36*, 297.
- (12) Lyon, E. J.; Georgakaki, I. P.; Reibenspies, J. H.; Darensbourg, M. Y. *J. Am. Chem. Soc.* **2001**, *123*, 3268.
- (13) Fauvel, K.; Mathieu, R.; Poilblanc, R. *Inorg. Chem.* **1976**, *15*, 976.
- (14) Savariault, J.-M.; Bonnet, J.-J.; Mathieu, R.; Galy, J. C. *R. Acad. Sci.* **1977**, *284*, C663.
- (15) (a) Kubas, G. J. *Acc. Chem. Res.* **1988**, *21*, 120. (b) Kubas, G. J. *Metal Dihydrogen and σ -Bond Complexes*; Kluwer Academic/Plenum Press: New York, 2001.
- (16) (a) De Lacey, A. L.; Stadler, C.; Cavazza, C.; Hatchikian, E. C.; Fernandez, V. M. *J. Am. Chem. Soc.* **2000**, *122*, 11232. (b) Chen, Z.; Lemon, B. J.; Huang, S.; Swartz, D. J.; Peters, J. W.; Bagley, K. A. *Biochemistry* **2002**, *41*, 2036.
- (17) (a) Popescu, C. V.; Münck, E. *J. Am. Chem. Soc.* **1999**, *121*, 7877. (b) Adams, M. W. *Biochim. Biophys. Acta* **1990**, *1020*, 115. (c) Bennet, B.; Lemon, B. J.; Peters, J. W. *Biochemistry* **2000**, *39*, 7455.
- (18) Zhao, X.; Georgakaki, I. P.; Miller, M. L.; Yarbrough, J. C.; Darensbourg, M. Y. *J. Am. Chem. Soc.* **2001**, *123*, 9710.
- (19) Sellmann, D.; Geipel, F.; Moll, M. *Angew. Chem., Int. Ed.* **2000**, *39*, 561.
- (20) Sellmann, D.; Fürsattel, A. *Angew. Chem., Int. Ed.* **1999**, *38*, 2023.
- (21) Collman, J. P.; Wagenknecht, P. S.; Hembre, R. T.; Lewis, N. S. *J. Am. Chem. Soc.* **1990**, *112*, 1294.
- (22) Albeniz, A. C.; Heinekey, D. M.; Crabtree, R. H. *Inorg. Chem.* **1991**, *30*, 3632.
- (23) Chinn, M. S.; Heinekey, D. M. *J. Am. Chem. Soc.* **1987**, *109*, 5865.

- (24) Rocchini, E.; Rigo P.; Mezzetti, A.; Stephan, T.; Morris R. H.; Lough, A. J.; Forde, C. E.; Fong, T. P.; Drouin S. D. *J. Chem. Soc., Dalton Trans.* **2000**, 3591.
- (25) Ellgen, P. C.; Gerlach, J. N. *Inorg. Chem.* **1973**, *12*, 2526.
- (26) (a) Maresca, L.; Greggio, F.; Sbrignadello, G.; Bor, G. *Inorg. Chim. Acta* **1971**, *5*, 667. (b) De Beer, J. A.; Haines, R. J.; Greatrex, R.; Greenwood, N. N. *J. Organomet. Chem.* **1971**, *27*, C33. (c) Le Borgne, G.; Grandjean, D.; Mathieu, R.; Poilblanc, R. *J. Organomet. Chem.* **1977**, *131*, 429.

Table 1. Infrared Data of the Fe₂S₂ Derivatives in the Carbonyl Stretching Frequency Region (CH₃CN Solutions unless Otherwise Indicated)

compound ^a	$\nu(\text{CO}), \text{cm}^{-1}$
[(<i>μ</i> -SEt)Fe(CO) ₂ (PMe ₃) ₂] (1)	1977(s), 1931(m), 1908(s)
(<i>μ</i> -edt)[Fe(CO) ₂ (PMe ₃) ₂] (2)	1982(s), 1944(s), 1908(s), 1896(m, br)
(<i>μ</i> -pdt)[Fe(CO) ₂ (PMe ₃) ₂] (3)	1979(m), 1942(s), 1898(s)
(<i>μ</i> - <i>o</i> -xyldt)[Fe(CO) ₂ (PMe ₃) ₂] (4)	1983(m), 1948(s), 1903(s)
(<i>μ</i> -pdt)[Fe(CO) ₂ (PMe ₂ Ph) ₂] (5)	1982(ms), 1946(s), 1910(ms)
<i>syn</i> -(<i>μ</i> -SCH ₂ CH ₂ PPh ₂) ₂ Fe ₂ (CO) ₄ (6)	1985(m), 1960(s), 1910(s), 1903(sh) ^b
<i>anti</i> -(<i>μ</i> -SCH ₂ CH ₂ PPh ₂) ₂ Fe ₂ (CO) ₄ (7)	1981(w), 1960(s), 1912(s), 1904(sh) ^b
{(<i>μ</i> -H)[(<i>μ</i> -SEt)Fe(CO) ₂ (PMe ₃) ₂] ⁺ [PF ₆] ⁻ (1-H⁺)	2046(s), 2025(ms), 1990(s)
{(<i>μ</i> -H)(<i>μ</i> -edt)[Fe(CO) ₂ (PMe ₃) ₂] ⁺ [PF ₆] ⁻ (2-H⁺)	2034(s), 1994(s)
{(<i>μ</i> -H)(<i>μ</i> -pdt)[Fe(CO) ₂ (PMe ₃) ₂] ⁺ [PF ₆] ⁻ (3-H⁺)	2029(s), 1989(s)
{(<i>μ</i> -H)(<i>μ</i> - <i>o</i> -xyldt)[Fe(CO) ₂ (PMe ₃) ₂] ⁺ [PF ₆] ⁻ (4-H⁺)	2034(s), 1992(m)
{(<i>μ</i> -H)(<i>μ</i> -pdt)[Fe(CO) ₂ (PMe ₂ Ph) ₂] ⁺ [PF ₆] ⁻ (5-H⁺)	2034(s), 1992(s)
[(<i>μ</i> -H)(<i>syn</i> -(<i>μ</i> -SCH ₂ CH ₂ PPh ₂) ₂ Fe ₂ (CO) ₄) ⁺ [CF ₃ SO ₃] ⁻ (6-H⁺)	2049(sh), 2039(s), 1995(m, br) ^b
[(<i>μ</i> -H)(<i>anti</i> -(<i>μ</i> -SCH ₂ CH ₂ PPh ₂) ₂ Fe ₂ (CO) ₄) ⁺ [CF ₃ SO ₃] ⁻ (7-H⁺)	2053(m), 2033(s), 2000(m, br) ^b

^a edt = SCH₂CH₂S; *o*-xyldt = SCH₂C₆H₄CH₂S. ^b THF solution.

substituent P-donor ligands are designated as apical and basal, resulting in the four possible conformations shown. In this manuscript, the ap/ba designations are retained for the protonated complexes, **n-H⁺**, even though the iron atoms in the resultant bridging hydrides are in octahedral coordination environments.

Experimental Section

Materials and Techniques. All manipulations were performed using standard Schlenk-line and syringe/rubber septa techniques under N₂ or in an argon atmosphere glovebox. Solvents were of reagent grade and purified as follows: Dichloromethane was distilled over P₂O₅ under N₂. Acetonitrile was distilled once from CaH₂ and once from P₂O₅, and then freshly distilled from CaH₂ immediately before use. Diethyl ether, toluene, THF, and hexane were distilled from sodium/benzophenone under N₂. The following materials were of reagent grade and used as received: Fe₃(CO)₁₂, 1,3-propanedithiol, 1,2-ethanedithiol, ethanethiol, 1,2-benzene-dimethanethiol, PMe₃, PMe₂Ph, concentrated HCl and NH₄PF₆ (Aldrich Chemical Co.), and deuterated solvents and D₂ (Cambridge Isotope Laboratories).

Infrared spectra were recorded on an IBM IR/32 using a 0.1 mm NaCl cell or on a ReactIR 1000 system from Applied Systems Inc., equipped with an MCT detector and 30 bounce SiCOMP in situ probe. ¹H, ¹³C, and ³¹P NMR (85% H₃PO₄ was used as external reference) spectra were recorded on a Unity+ 300 MHz superconducting NMR instrument operating at 299.9, 75.43, and 121.43 MHz, respectively. ²H NMR spectra were recorded on a Unity Inova-400 NMR instrument with a 5 mm autoswitchable probe operating at 61.35 MHz.

Preparations. Full descriptions of syntheses and characterizations are presented in Supporting Information.

(*μ*-SRS)[Fe(CO)₂(PMe₃)₂]. The dinuclear iron hexacarbonyl compounds, (*μ*-SRS)Fe₂(CO)₆, were synthesized according to literature methods.⁵ The PMe₃ derivatives of these compounds were prepared by refluxing excess PMe₃ with the corresponding (*μ*-SRS)-Fe₂(CO)₆ in hexane until the starting compound was consumed as indicated by IR. The solution was then filtered through Celite, and analytically pure compounds were obtained after removal of solvent and excess PMe₃ by vacuum. The (*μ*-pdt)[Fe(CO)₂(PMe₂Ph)₂] was prepared in similar fashion, with yields on the order of 60–90%. Crystals suitable for X-ray analysis were obtained by evaporative concentration of hexane solutions. The $\nu(\text{CO})$ IR positions of the series of neutral complexes and the hydrides in THF or CH₃CN are given in Table 1. Positions in other solvents are listed in Supporting Information.

{(*μ*-H)(*μ*-SRS)[Fe(CO)₂(PMe₃)₂]⁺[PF₆]⁻. According to the literature,¹³ a typical preparation is presented here. To a methanol solution of (*μ*-SRS)[Fe(CO)₂(PMe₃)₂] was added excess concentrated HCl forming a red-orange solution. A red or yellow-orange solid precipitated upon addition of a saturated aqueous solution of NH₄PF₆ to the solution. The solid was filtered and washed first with water and then ether to remove any starting material; yields were on the order of 50–60%. Crystals suitable for X-ray studies were obtained by slow diffusion of hexanes into CH₂Cl₂ or MeOH solutions of the hydrides.

H/D Exchange Reactions. The H/D exchange reactions of all hydrides were carried out as ~0.10 M solutions in medium-pressure NMR tubes (Wilmad, 528-PV-7) as PF₆⁻ or -SO₃CF₃ salts. The hydrides were dissolved in CH₂Cl₂ and then transferred to the degassed, N₂-filled NMR tubes. Before pressurizing with D₂ or H₂, the tubes were gently degassed under vacuum. The tubes were then irradiated either by exposure to sunlight by placing on the window sill, to ambient laboratory light, or to irradiation from a sunlamp (65 W, 120 V, PLANT GRON SHOW 65BR30/PL). The growth of (*μ*-D)Fe₂⁺ and decrease of (*μ*-H)Fe₂⁺ were monitored by ²H NMR or ¹H NMR, respectively.

Competition Reactions of H/D Exchange. Equal moles of different hydrides (50–60 mg, ca. 0.1 mmol) were dissolved together in ~0.8 mL CH₂Cl₂ and transferred to an NMR tube. Following the procedure described previously, the growth of (*μ*-D)Fe₂⁺ for each hydride was monitored by ²H NMR. Integration of the high-field signal intensities established relative H/D exchange rates.

Catalytic Formation of HD from H₂ and D₂. A 10 mg (0.016 mmol) portion of {(*μ*-H)(*μ*-pdt)[Fe(CO)₂(PMe₃)₂]⁺[PF₆]⁻ was dissolved in 1.0 g of CD₂Cl₂ and transferred to the NMR tube. This tube was first pressurized with 6 bar H₂ and then with D₂ to a total of 12 bar (ca. 0.5 mmol H₂ and D₂). The tube was placed in the sunlight, and ¹H NMR spectra were taken at time intervals to follow the growth of HD from H₂ and D₂.

H/D Exchange between D₂O and 3-H⁺. To a CH₂Cl₂ solution of **3-H⁺** (60 mg, 0.094 mmol) in an NMR tube was added 1, 2, 3, and 4 μL of D₂O; ²H NMR spectra of the sample were taken after each addition of D₂O. The tube was then left in the dark overnight and the spectrum taken again before and after exposure to sunlight.

H/D Exchange between H₂O and D₂. To an NMR tube containing a CH₂Cl₂ solution of **3-H⁺** (60 mg, 0.094 mmol) was added 2 μL (0.11 mmol) of H₂O. The NMR tube was then pressurized with 10 bar D₂ and kept in the dark for 12 h. The ²H NMR spectra of this sample were recorded before and after exposure to sunlight for 2 h and for 10 h.

Comparisons of Stability of Hydrides in CH₂Cl₂ Solutions. Hydride salts were weighed out (ca. 0.1 mmol) in an Ar-filled

glovebox, and each was dissolved in 2 mL of CH_2Cl_2 . The hydride solutions were transferred to a medium-pressure NMR tube. A reference $\nu(\text{CO})$ IR spectrum of each sample was taken prior to pressurizing the NMR tubes to 7.5 bar H_2 and placing side by side in the sunlight. The pressure was released, and samples for IR measurements were withdrawn after 1, 2, 3, and 5 days. Repressurization to 7.5 bar was required before continuation of the irradiation experiment.

In Situ Monitor of Stability of $\{(\mu\text{-H})(\mu\text{-pdt})[\text{Fe}(\text{CO})_2(\text{PMe}_3)_2]\}_2^+[\text{PF}_6]^-$ in CH_3CN and in CH_2Cl_2 . A 0.20 g sample of $\{(\mu\text{-H})(\mu\text{-pdt})[\text{Fe}(\text{CO})_2(\text{PMe}_3)_2]\}_2^+[\text{PF}_6]^-$ was dissolved in 30 mL of CH_3CN or CH_2Cl_2 and transferred to the reaction vessel of the ReactIR. IR spectra were taken every 1 min over the course of 5 h (CH_3CN) or every 2 min for 10 h (CH_2Cl_2) while the solution was being magnetically stirred and irradiated by a sunlamp.

Computational Details. The structures of examined complexes were optimized using density functional theory (DFT)²⁷ with the Becke3 parameter hybrid exchange functional²⁸ and LYP correlation functional²⁹ (B3LYP). All calculations were performed using Gaussian 98 programs,³⁰ using a Dunning basis set of double- ζ quality for C, H, and O atoms.³¹ A modified version of the Hay and Wadt double- ζ basis set with effective core potentials (ECP)³² was used for Fe atoms taken from the work of Couty and Hall.³³ A polarization function optimized for the double- ζ basis set and ECPs of Hay and Wadt³² were used for S and the P atoms taken from the work of Höllwarth et al.³⁴

X-ray Structure Determination. The X-ray data were collected on a Bruker Smart 1000 CCD diffractometer or a Bruker Apex CCD diffractometer and covered a hemisphere of reciprocal space by a combination of three sets of exposures. The space groups were determined on the basis of systematic absences and intensity statistics. The structures were solved by direct methods. Anisotropic displacement parameters were determined for all non-hydrogen atoms. Hydrogen atoms were placed at idealized positions and refined with fixed isotropic displacement parameters. The following is a list of programs used: for data collection and cell refinement, SMART;³⁵ data reduction, SAINTPLUS;³⁶ structure solution,

(27) Parr, R. G.; Yang, W. *Density-functional theory of atoms and molecules*; Oxford University Press: Oxford, 1989.

(28) (a) Beck, A. D. *Phys. Rev. A* **1988**, *38*, 3098. (b) Beck, A. D. *J. Chem. Phys.* **1993**, *98*, 1372. (c) Beck, A. D. *J. Chem. Phys.* **1993**, *98*, 5648.

(29) (a) Lee, C.; Yang, W.; Parr, R. G. *Phys. Rev. B* **1988**, *37*, 785. (b) Miehlich, B.; Savin, A.; Stoll, H.; Preuss, H. *Chem. Phys. Lett.* **1989**, *157*, 200.

(30) Frisch, M. J.; Trucks, G. W.; Schlegel, H. B.; Scuseria, G. E.; Robb, M. A.; Cheeseman, J. R.; Zakrzewski, V. G.; Montgomery, J. A., Jr.; Stratmann, R. E.; Burant, J. C.; Dapprich, S.; Millam, J. M.; Daniels, A. D.; Kudin, K. N.; Strain, M. C.; Farkas, O.; Tomasi, J.; Barone, V.; Cossi, M.; Cammi, R.; Mennucci, B.; Pomelli, C.; Adamo, C.; Clifford, S.; Ochterski, J.; Petersson, G. A.; Ayala, P. Y.; Cui, Q.; Morokuma, K.; Malick, D. K.; Rabuck, A. D.; Raghavachari, K.; Foresman, J. B.; Cioslowski, J.; Ortiz, J. V.; Stefanov, B. B.; Liu, G.; Liashenko, A.; Piskorz, P.; Komaromi, I.; Gomperts, R.; Martin, R. L.; Fox, D. J.; Keith, T.; Al-Laham, M. A.; Peng, C. Y.; Nanayakkara, A.; Gonzalez, C.; Challacombe, M.; Gill, P. M. W.; Johnson, B. G.; Chen, W.; Wong, M. W.; Andres, J. L.; Head-Gordon, M.; Replogle, E. S.; Pople, J. A. *Gaussian 98*, revision A.7; Gaussian, Inc.: Pittsburgh, PA, 1998.

(31) (a) Dunning, T. H., Jr. *J. Chem. Phys.* **1970**, *53*, 2823. (b) Dunning, T. H., Jr.; Hay, P. J. *Methods of Electronic Structure Theory*; Plenum Press: New York, 1977, Vol. 3.

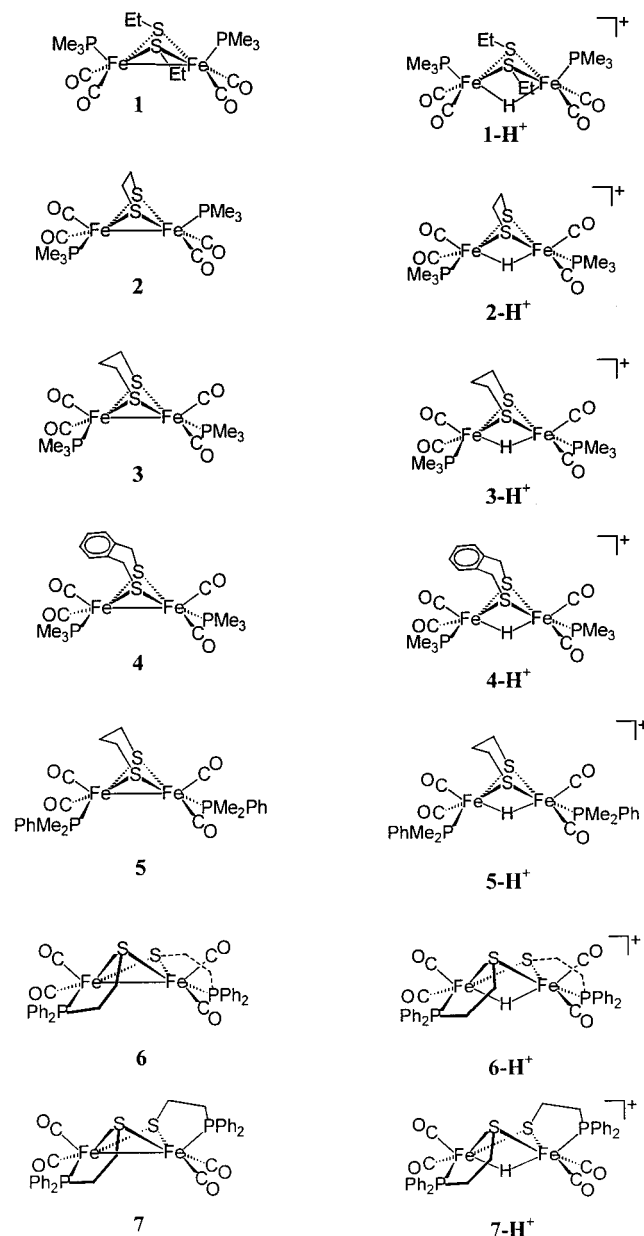
(32) (a) Hay, P. J.; Wadt, W. R. *J. Chem. Phys.* **1985**, *82*, 270. (b) Hay, P. J.; Wadt, W. R. *J. Chem. Phys.* **1985**, *82*, 284. (c) Hay, P. J.; Wadt, W. R. *J. Chem. Phys.* **1985**, *82*, 299.

(33) Couty, M.; Hall, M. B. *J. Comput. Chem.* **1996**, *17*, 1359.

(34) Höllwarth, A.; Böhme, M.; Dapprich, S.; Ehlers, A. W.; Gobbi, A.; Jonas, V.; Köhler, K. F.; Stegmann, R.; Veldkamp, A.; Frenking, G. *Chem. Phys. Lett.* **1993**, *208*, 237.

(35) SMART 1000 CCD; Bruker Analytical X-ray Systems: Madison, WI, 1999.

Chart 2



SHELXS-86 (Sheldrick);³⁷ structure refinement, SHELXL-97 (Sheldrick);³⁸ and molecular graphics and preparation of material for publication, SHELXTL-Plus, version 5.1 or later (Bruker).³⁹

Results and Discussion

Characterization of the Series: The Solid State. Shown in Chart 2 are the compounds used in this study along with designations adopted throughout. The stick drawings represent the conformers found in the solid-state structures, as determined by X-ray crystallography for all members of the series excepting compounds **5**, **6-H⁺**, and **4-H⁺**. Crystals of

(36) SAINT-Plus, version 6.02; Bruker: Madison, WI, 1999.

(37) Sheldrick, G. *SHELXS-86: Program for Crystal Structure Solution*; Institut für Anorganische Chemie der Universität: Göttingen, Germany, 1986.


(38) Sheldrick, G. *SHELXL-97: Program for Crystal Structure Refinement*; Institut für Anorganische Chemie der Universität: Göttingen, Germany, 1997.

(39) SHELXTL, version 5.1 or later; Bruker: Madison, WI, 1998.

Table 2. Crystallographic Data^a for Complexes **1**, **1-H⁺**, **2**, **2-H⁺**, **4**, and **5-H⁺**

	1	1-H⁺	2	2-H⁺	4	5-H⁺
empirical formula	C ₁₄ H ₂₈ Fe ₂ O ₄ P ₂ S ₂	C ₁₄ H ₂₉ F ₆ Fe ₂ O ₄ P ₃ S ₂	C ₁₀ H ₂₂ Fe ₂ O ₄ P ₂ S ₂	C ₁₀ H ₂₃ F ₆ Fe ₂ O ₄ P ₃ S ₂	C ₁₈ H ₂₆ Fe ₂ O ₄ P ₂ S ₂	C ₂₃ H ₂₉ F ₆ Fe ₂ O ₄ P ₃ S ₂
fw	498.12	644.1	468.06	614.03	544.15	752.19
cryst syst	triclinic	monoclinic	monoclinic	monoclinic	monoclinic	triclinic
space group	<i>P</i> $\bar{1}$	<i>P</i> 2 ₁ / <i>c</i>	<i>P</i> 2 ₁ / <i>c</i>	<i>C</i> 2/ <i>c</i>	<i>P</i> 2 ₁ / <i>n</i>	<i>P</i> $\bar{1}$
unit cell						
<i>a</i> (Å)	10.474(2)	10.3731(9)	14.560(2)	25.837(3)	10.6231(11)	9.9108(12)
<i>b</i> (Å)	14.233(3)	12.5853(11)	10.3348(15)	17.3690(18)	18.8448(19)	10.0961(12)
<i>c</i> (Å)	15.932(3)	20.2228(17)	13.2183(19)	22.502(2)	12.3312(13)	15.8252(18)
α (deg)	75.656(4)					98.283(2)
β (deg)	89.180(4)	98.0290(10)	99.743(3)	116.039(2)	111.464(2)	107.219(2)
γ (deg)	86.004(4)					96.810(2)
<i>V</i> (Å ³)	2295.6(8)	2614.2(4)	1960.3(5)	9073.2(16)	2297.4(4)	1474.8(3)
<i>Z</i>	4	4	4	16	4	2
<i>d</i> (calcd), g/cm ³	1.441	1.637	1.586	1.798	1.573	1.694
R1 ^b [<i>I</i> > 2 σ (<i>I</i>)]	0.0453	0.0278	0.0529	0.0751	0.0366	0.0679
wR2 ^c	0.1159	0.071	0.1391	0.1743	0.0951	0.1716

^a Obtained using graphite-monochromatized Mo K α radiation ($\lambda = 0.71073$ Å) at 110(2) K for all structures. ^b R1 = $\sum||F_o| - |F_c||/\sum F_o$. ^c wR2 = $[\sum[w(F_o^2 - F_c^2)^2]/\sum w(F_o^2)^2]^{1/2}$.

Table 3. Selected Metric Data for Binuclear Iron Phosphino Carbonyls Bridged by Thiolates


	1	1-H⁺	2	2-H⁺	3	3-H⁺	4	5-H⁺	6	7	7-H⁺
Fe...Fe	2.5097(7)	2.5708(4)	2.5159(6)	2.5742(13)	2.555(2)	2.5784(8)	2.5825(7)	2.5859(7)	2.603(2)	2.5621(7)	2.580(1)
Fe-H	N/A	1.66(2)	N/A	1.69(6)	N/A	1.710(14)	N/A	1.58(6)	N/A	N/A	1.664(6)
Fe-P _{ap}	2.219(1) ^a	2.2366(6) ^a	2.2075(8)	N/A	N/A	N/A	N/A	N/A	N/A	2.2153(8)	2.236(1)
Fe-P _{ba}	N/A	N/A	2.2212(8)	2.2392(16)	2.234(3)	2.2523(12)	2.2207(10)	2.2543(11)	2.209(2)	2.2142(8)	2.223(1)
Fe-C _{CO,ap}	N/A	N/A	1.769(3)	1.774(6)	1.772(9)	1.779(4)	1.771(4)	1.776(4)	1.782(8)	1.778(2)	1.789(5)
Fe-C _{CO,ba}	1.7552(3) ^d	1.778(3) ^d	1.759(3) ^b	1.770(6)	1.742(10)	1.778(4)	1.760(4)	1.800(4)	1.753(8)	1.762(3)	1.793(5)
Fe-S _{μ-SR^c}	2.280(1)	2.2793(7)	2.2521(8)	2.2562(16)	2.254(2)	2.2717(11)	2.252(1)	2.2678(11)	2.265(2)	2.2581(8)	2.266(1)
Fe dsp ^e	0.315	0.180	0.365	0.197	0.376	0.231	0.360	0.209	0.303	0.329	0.180
S...S	2.798	2.808	2.897	2.924	3.026	3.064	3.107	3.064	2.826	2.945	2.969
dihedral ^f (deg)	94.6	96.5	101.7	104.2	109.2	109.9	114.7	110.6	99.3	104.7	105.6
Fe-S-Fe (deg)	66.78(3)	68.66(2)	67.91(2)	69.57(5)	69.06(8)	69.15(4)	69.98(3)	69.52(3)	70.15(7)	69.12(3)	69.39(8)
S-Fe-S (deg)	75.70(3)	76.04(2)	80.06(3)	80.78(6)	84.34(11)	84.77(4)	87.22(3)	85.00(4)	77.18(8)	86.54(3)	81.84(10)
L _{ap} -Fe-L _{ba} (deg)	98.99(11)	93.86(7)	97.2(1)	94.8(4)	96.8(4)	93.91(16)	96.93(14)	93.06(15)	98.15(3)	100.32(9)	96.42(4)
L _{ap} -Fe-S (deg)	99.45(3)	96.82(2)	103.70(6)	95.9(2)	104.0(3)	98.70(13)	102.94(12)	98.36(13)	99.22(3)	114.93(7)	93.34(20)

^a Average over two Fe-P_{ap} bonds. ^b Average over three Fe-C_{CO,ba} bonds. ^c Average over four Fe-S _{μ -SR} bonds. ^d Average over four Fe-C_{CO,ba} bonds. ^e Fe dsp = Displacement of Fe from best plane of S₂L_(ba)2 toward L_{ap}. ^f Defined by the intersection of the two SFe₂ planes.

the latter hydride were twinned, and while metric data are not reliable, the positions of the phosphine ligands are certain. Furthermore, analyses of solution NMR data, vide infra, corroborate the structural assignments of all as given in Chart 2. Crystallographic data are given in Table 2, listings of selected metric data are given in Table 3, and full structure reports are available in Supporting Information. The molecular structures of complexes **1** and **1-H⁺**, **2** and **2-H⁺**, **4**, and **5-H⁺** are shown as ball-and-stick representations in Figures 2–5, respectively. Details of the structures of **3**, **3-H⁺**, **6**, **7**, and **7-H⁺** were presented elsewhere.^{18,40}

The S–C orientations of all compounds containing the S to S linked bridges are necessarily of the syn' orientation, and with one exception, all these compounds have the PMe₃ or PMe₂Ph ligands in the ba/ba (transoid) conformation and are cis to the Fe^I–Fe^I bond or Fe^{II}(μ -H)Fe^{II} units. That exception is complex **2**, which, with the simplest of S to S

links and a minimum of steric hindrance at the bridge, finds the PMe₃ ligands in the ap/ba arrangement. Nevertheless, on protonation, the resulting **2-H⁺** hydride conforms to the ba/ba (transoid) orientation adopted by all other *n*-H⁺ complexes in this class. The **1** and **1-H⁺** pair of complexes shows a marked contrast. In agreement with an earlier study on SMe bridged complexes,^{26c} the S–C bond is in the syn conformation which exacts steric hindrance on the basal coordination positions about iron and directs the PMe₃ ligands into apical sites, trans to the Fe^I–Fe^I bond or Fe^{II}(μ -H)Fe^{II} units.

Each bridging thiolate in complexes **6**, **7**, and **7-H⁺** is connected to the P-donor site via an ethylene unit.⁴⁰ Complex **6** has a syn conformation at the S–C bonds, which directs the chelated PPh₂ donors in the ba/ba (transoid) positions. For **7** and **7-H⁺**, the anti arrangement of the S–C bonds ensures that one P-donor goes to the apical and one to the basal positions in the Fe(CO)₂P termini. Thus, the arrangement of P-donors in complex **7** is the same as that in complex **2**.

(40) Zhao, X.; Hsiao, Y.-M.; Lai, C.-H.; Reibenspies, J. H.; Darensbourg, M. Y. *Inorg. Chem.* **2002**, *41*, 699.

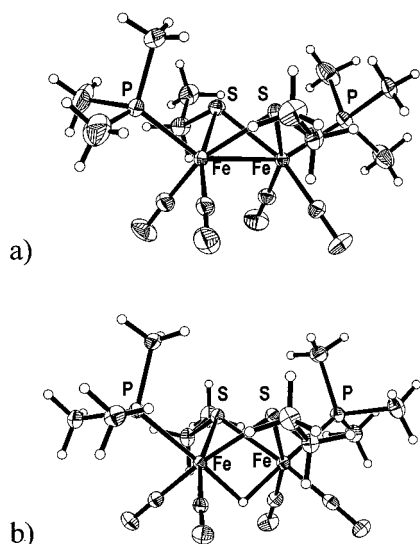


Figure 2. Thermal ellipsoid representations (50% probability) of the molecular structures of (a) $[(\mu\text{-SEt})\text{Fe}(\text{CO})_2\text{PMe}_3]_2$, **1**, and (b) $(\mu\text{-H})[(\mu\text{-SEt})\text{Fe}(\text{CO})_2\text{PMe}_3]_2^+$, **1-H⁺**.

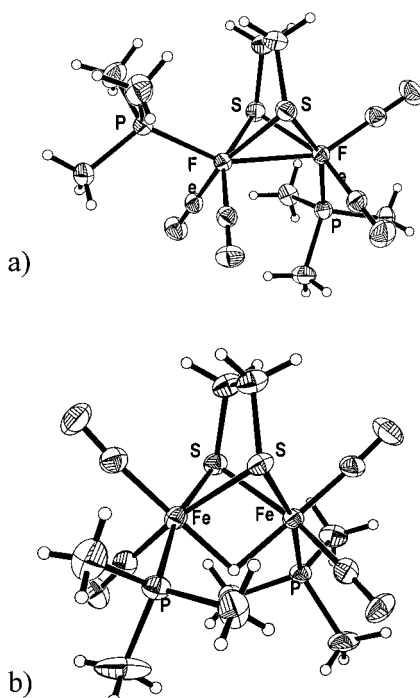


Figure 3. Thermal ellipsoid representations (50% probability) of the molecular structures of (a) $(\mu\text{-edt})[\text{Fe}(\text{CO})_2\text{PMe}_3]_2$, **2**, and (b) $(\mu\text{-H})(\mu\text{-edt})[\text{Fe}(\text{CO})_2\text{PMe}_3]_2^+$, **2-H⁺**.

The $\text{Fe}\cdots\text{Fe}$ distances, Table 3, range from 2.51 to 2.60 Å in the neutral complexes in which there is an $\text{Fe}\text{--}\text{Fe}$ bond; they show slight increases on the order of 0.02–0.05 Å on protonation to produce the bridging hydride complexes. The $\mu\text{-SEt}$ bridged species **1** and **1-H⁺** show the greatest difference in $\text{Fe}\text{--}\text{Fe}$ distance; nevertheless, they are approximately an order of magnitude less than changes observed on protonation of nonsupported metal–metal bonds.⁴¹ The small increase in $\text{Fe}\text{--}\text{Fe}$ distance reflects the minor structural rearrangement resulting from changing an edge-bridged bi-square-pyramid into a face-bridged bi-octahedron.

(41) Nataro, C.; Angelici, R. J. *Inorg. Chem.* **1998**, *37*, 2975.

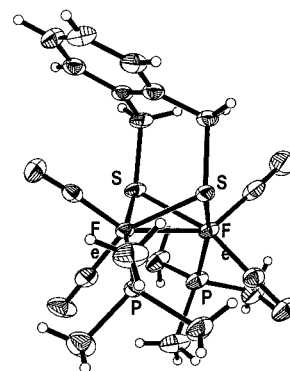


Figure 4. Thermal ellipsoid representations (50% probability) of the molecular structure of $(\mu\text{-oxy})[\text{Fe}(\text{CO})_2\text{PMe}_3]_2$, **4**.

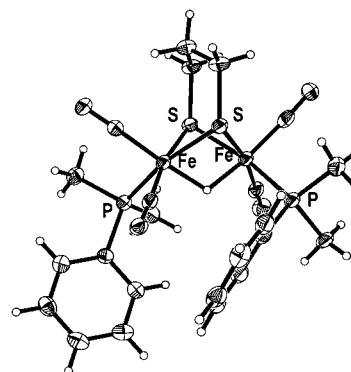


Figure 5. Thermal ellipsoid representations (50% probability) of the molecular structure of $(\mu\text{-H})(\mu\text{-pdt})[\text{Fe}(\text{CO})_2\text{PMe}_2\text{Ph}]_2^+$, **5-H⁺**.

The $\text{Fe}\text{--}\text{P}$ and $\text{Fe}\text{--}\text{C}$ bond distances show very slight increases following protonation while the $\text{Fe}\text{--}\text{S}$ distances are statistically indistinguishable. Because in the protonated derivatives the formal oxidation state of iron increases to +2, the consistency in $\text{Fe}\text{--}\text{P}$ or $\text{Fe}\text{--}\text{S}$ distances is evidence for the stereochemical integrity of the hydride ligand. That is, the increase in coordination number about the iron (which should increase the $\text{M}\text{--}\text{L}$ distance) compensates for the increased charge on iron (which should decrease the $\text{M}\text{--}\text{L}$ distance).

While still minor, the largest metric differences within the series are in the S to S “wing-tip” distances. The SEt derivatives **1** and **1-H⁺** are ca. 0.1 Å closer together than are the S to S linked complexes which spread the wing-tips according to the organic linker size. Complex **6** which has the $\text{S}\text{--}\text{P}$ chelated $\text{S}\text{--}\text{CH}_2$ in syn arrangement is similar to complex **1**. In each pair of structurally characterized n and $n\text{-H}^+$ compounds, there is seen a decrease in the displacement of Fe from the $\text{S}_2(\text{CO})\text{L}$ planes ($\text{L} = \text{CO}$ or PR_3) toward the apical ligand from an average of 0.35 Å in the neutral, $\text{Fe}\text{--}\text{Fe}$ bonded complexes to ca. 0.20 Å in the bridging hydrides.

Computational Results. The molecular structures of **3** and **3-H⁺** determined by X-ray crystallography are supported by DFT computations. As indicated in Figure 6a, the HOMO of **3** is characterized by a large lobe underneath the Fe_2S_2 frame representing the electron density of the metal–metal bond, symmetrically distributed as indicated by Mulliken charges on both iron atoms of -1.07 . The optimized $\text{Fe}\text{--}\text{Fe}$ distance of 2.548 Å is in good agreement with that from

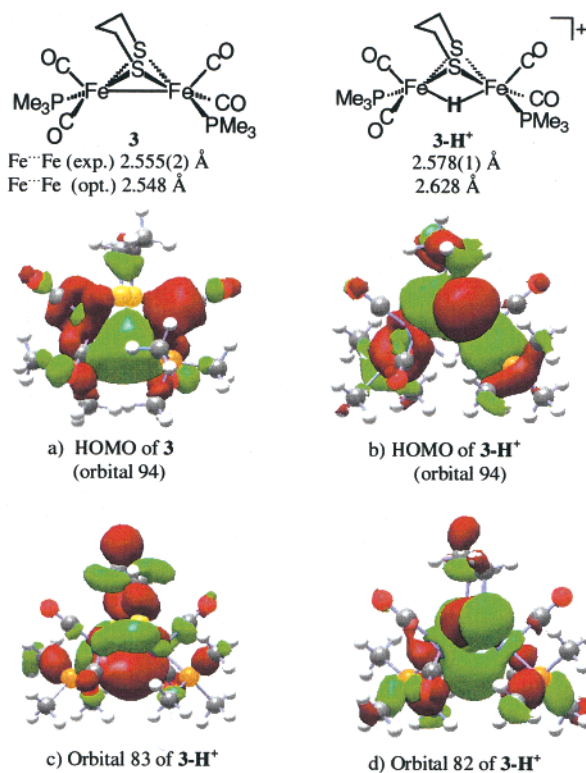


Figure 6. HOMOs of complexes **3** and **3-H⁺**: (a) HOMO (orbital 94) of complex **3**; (b) HOMO (orbital 94) of complex **3-H⁺**; (c) and (d) orbitals 83 and 82 of **3-H⁺** illustrating primarily hydride-based electron density.

the crystal structure, 2.555(2) Å. For the protonated complex, DFT computations find the Fe...Fe distance to be 2.648 Å (experimental = 2.578(1) Å), and the HOMO (orbital 94, Figure 6b) has a prominent S-component. The electron density identified as hydride-based is stabilized in orbitals 83 and 82, Figure 6c and 6d, respectively.

Solution Structure and Fluxional Characteristics. Space filling models indicate that the syn-ap/ap combination seen in complexes **1** and **1-H⁺** minimizes steric interactions between S-Et and PMe₃, while such an ap/ap positioning of PMe₃ ligands in **3**, **4**, and **6** would exact greater steric repulsions between substituent ligands and the S to S linked dithiolate. Hence, the observed structures represent sterically favored forms. The role of electronics in conformer stability, that is, whether there is an electronic preference for the better donor ligand to be cis or trans to the Fe–Fe bond density or the Fe(μ -H)Fe, is not clear. The observation of the ap/ba arrangement of the P-donor ligands of complex **2** suggests the thermodynamic preference is minimal and perhaps within the dictates of crystal packing forces. Indeed, variable temperature NMR data confirm ligand site exchange and rotation of the Fe(CO)₂PMe₃ units, *vide infra*.

Infrared Data. While oxidative addition of a proton to the Fe–Fe bond barely perturbs the structures of the *n* and *n-H⁺* series, the shift in metal–metal bond density to the hydride ligand and the development of positive charge on iron is most clearly indicated by the vibrational spectra of the CO reporter ligands. The solution infrared spectra of the neutral complexes in the $\nu(\text{CO})$ region show minor differences that are consistent with the symmetry of the complexes found in the solid-state X-ray crystal structures, Table 1.

Infrared spectra of the protonated, cationic complexes in the $\nu(\text{CO})$ region show an increase in average $\nu(\text{CO})$ values of ca. 70–90 cm⁻¹ over their neutral conjugate bases. Also notable is the simplification of the $\nu(\text{CO})$ IR spectra on going from the neutral to the protonated or bridging hydride complexes; the latter typically show only two absorptions, indicating electronic isolation or lack of electronic coupling of the discrete Fe^{II} units in the *n-H⁺* complexes. There are minor, but complicated, $\nu(\text{CO})$ wavenumber differences which depend on the P-donor ligand as well as on the S–R orientation.^{26a}

NMR Data and Variable Temperature Studies. Listed in Table 4 are chemical shift values for the bridging hydride complexes. A notable feature of the $J_{\text{H-P}}$ values is the small, 3–5 Hz, P to H coupling constant for the trans position of hydride and phosphorus seen in complexes **1-H⁺** and **7-H⁺**. All other $J_{\text{H-P}}$ values are in the range 19–24 Hz and characterize the cis orientation of the hydride and the phosphines. The $J_{\text{P-D}}$ values are about 1/7 of the $J_{\text{P-H}}$ values as predicted from the ratio of the magnetogyric ratios (γ) of H (26.75 rad T⁻¹ s⁻¹) and D (4.106 rad T⁻¹ s⁻¹).

Variable temperature (VT) NMR spectroscopy revealed the intramolecular site exchanges that are associated with (μ -pdt)[Fe(CO)₂(PMe₃)₂]₂ and {(μ -H)(μ -pdt)[Fe(CO)₂(PMe₃)₂]₂}⁺. The ¹H NMR spectra showed that the fluxionality of the propanedithiolate bridge that was observed in (μ -pdt)[Fe(CO)₂(PMe₃)₂]₂^{12,42} holds in the neutral disubstituted PMe₃ derivative as well as in the protonated complex (Figure 7a), with a similar coalescence temperature, approximately –60 °C. Variable temperature ¹³C NMR spectra in the CO region show that the CO site exchange is localized in the individual Fe(CO)₂(PMe₃) units in the neutral compound, again analogous to the CO site exchange of (μ -pdt)[Fe(CO)₂(PMe₃)₂]₂.¹² The lack of this pyramidal rotor feature in the protonated species is consistent with higher barriers in octahedral coordination environments of the Fe^{II} centers, Figure 7b, as compared to the pentacoordinate precursor.

For complex **2**, the temperature-dependent ³¹P NMR spectra show a single resonance at 22.0 ppm at room temperature, in agreement with the known fluxionality of the Fe(CO)₂L rotors in such complexes, *vide supra*.¹² On lowering the temperature, coalescence is observed at ca. –60 °C, and two new signals appear at 28.6 and 17.6 ppm, consistent with the ap/ba conformer in the solid-state structure of **2**. For complex **3**, the single ³¹P resonance is due to the equivalence of the P-donor sites according to their position and to the rapid interconversion of the iron-dithia-cyclohexane rings. On achieving the stopped-exchange region for the latter, two ³¹P resonances are observed, at 29.6 and 25.7 ppm, resulting from the slightly different chemical environments imposed by the fixed S to S bridge (Figure 7b). An isomer of complex **3** was noted by low intensity resonances which coalesced and reappeared as two small broad peaks as the temperature was lowered.

H/D Exchange Studies: H/D Exchange Reaction between *n-H⁺* and D₂. The experimental protocol established

(42) Winter, A.; Zsolnai, L.; Huttner, G. Z. *Naturforsch.* **1982**, *37b*, 1430.

Table 4. ^1H and ^2H NMR Spectral Data for $(\mu\text{-H})(\mu\text{-SR})_2[\text{Fe}(\text{CO})_2\text{PMe}_3]_2^+$ Complexes in CD_2Cl_2 as PF_6^- Salts unless Otherwise Noted

complex	$\mu\text{-H}^a$ (δ , ppm)	$J_{\text{P-H}}$ (Hz)	$\mu\text{-D}$ (δ , ppm)	$J_{\text{P-D}}$ (Hz)
$(\mu\text{-H})(\mu\text{-SEt})_2[\text{Fe}(\text{CO})_2\text{PMe}_3]_2^+$, 1-H ⁺	-15.79	3.6	-15.9 (-15.65, -15.7)	br
$(\mu\text{-H})(\mu\text{-edt})[\text{Fe}(\text{CO})_2\text{PMe}_3]_2^+$, 2-H ⁺	-17.32	22.8	-17.45	3.54
$(\mu\text{-H})(\mu\text{-pdt})[\text{Fe}(\text{CO})_2\text{PMe}_3]_2^+$, 3-H ⁺	-15.2	22	-15.3	3.31
$(\mu\text{-H})(\mu\text{-o-xyldt})[\text{Fe}(\text{CO})_2\text{PMe}_3]_2^+$, 4-H ⁺	-15.06	21.2	-15.17	3.07
$(\mu\text{-H})(\mu\text{-pdt})[\text{Fe}(\text{CO})_2\text{PMe}_2\text{Ph}]_2^+$, 5-H ⁺	-15.0	21.9	-15.1	3.31
$(\mu\text{-H})(\text{syn-}\mu\text{-SCH}_2\text{CH}_2\text{PPh}_2)[\text{Fe}(\text{CO})_2]_2^+$, 6-H ⁺ ^c	-17.5	21.4	-17.6	3.25
$(\mu\text{-H})(\text{anti-}\mu\text{-SCH}_2\text{CH}_2\text{PPh}_2)[\text{Fe}(\text{CO})_2]_2^+$, 7-H ⁺ ^c	-16.9	24/4.6 ^b	-17.0	3.56/n.o. ^b

^a All split as triplet, except for **7-H**⁺. ^b The larger coupling constant assigned to the cis Ph_2PCH_2 ; the smaller to the trans. ^c As OTf^- salts.

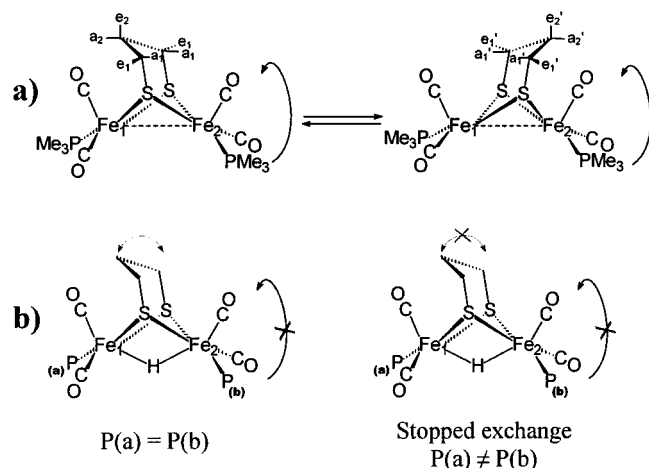


Figure 7. Fluxional characteristics of $(\mu\text{-pdt})[\text{Fe}(\text{CO})_2(\text{PMe}_3)_2]$ (**3**) and $\{(\mu\text{-H})(\mu\text{-pdt})[\text{Fe}(\text{CO})_2(\text{PMe}_3)_2]\}^+$ (**3-H**⁺).

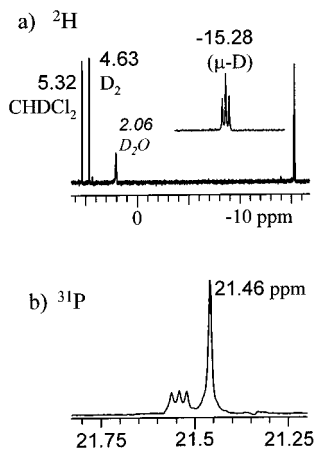


Figure 8. (a) ^2H NMR and (b) ^{31}P NMR spectra of D_2 -enriched **3-H**⁺, 8 bar D_2 in CH_2Cl_2 .

by Sellmann and others was followed.^{19–23} Typically, CH_2Cl_2 solutions of each hydride, **1-H**⁺ through **7-H**⁺, were placed in medium-pressure NMR tubes which were pressurized with D_2 (7–12 bar) and exposed to sunlight. H/D exchange into the bridging hydride position of $n\text{-H}^+$ and D_2 occurred in all as indicated by ^2H NMR. For example, H/D exchange between **3-H**⁺ and D_2 in CH_2Cl_2 solution resulted in the formation of **3-D**⁺, which showed up as a triplet at -15.28 ppm in the high field region of the ^2H NMR with $J_{\text{P-D}} = 3.32$ Hz, Figure 8a. After long reaction periods, a minor resonance (<5%), a doublet centered at 6.29 ppm with coupling constant of 72.9 Hz, was also observed and assigned to DPMe_3^+ . A complete listing of the bridging hydride and deuteride chemical shifts is given in Table 4. The H/D

exchange reaction was corroborated by the H-decoupled ^{31}P NMR spectrum, Figure 8b, which showed a small triplet at 21.54 ppm resulting from the coupling between P and $(\mu\text{-D})\text{Fe}_2^+$ with the same coupling constant (3.32 Hz) as that obtained from the ^2H NMR. Another single peak at 21.46 ppm is due to the H-decoupled ^{31}P signal from $(\mu\text{-H})\text{Fe}_2^+$, Figure 8b.

The H/D exchange reaction between $(\mu\text{-H})\text{Fe}_2^+$ and D_2 is affected by several factors, including light, solvent, added ligands, and counterion. The following control experiments are described for **3-H**⁺ [PF_6^-]; however, all complexes behaved similarly.

(1) Light. When a CH_2Cl_2 solution of **3-H**⁺ under the presence of D_2 (10 bar) was left in the dark at 22 °C for 4–6 days, there was no indication of the formation of **3-D**⁺. Both natural and artificial light sources promoted the reaction, and the rate or extent of the reaction over time depended on the strength of the light source.

(2) Solvent. The optimal solvent for H/D exchange studies in terms of solubility, stability, and activity was CH_2Cl_2 . Nevertheless, a small amount of solid formed at the bottom of NMR tubes during the photoassisted H/D exchange reaction. The solution IR spectra of the photolyzed samples in the $\nu(\text{CO})$ region were identical to those of the original sample; the residue showed no $\nu(\text{CO})$ bands. In acetonitrile, the decomposition process was obvious and extensive on exposure to sunlight for 0.5 h, showing color changes from red-orange to red-brown. There was no H/D exchange activity in the decolorized sample in acetonitrile, and the ^1H and ^2H NMR spectra showed the formation of other hydride species in the range -6 to -10 ppm. The high field resonances are attributed to $\text{CH}_3\text{CN}/\text{CO}$ substitution products, $\{(\mu\text{-H})(\mu\text{-pdt})[\text{Fe}_2(\text{CO})_{4-x}(\text{CH}_3\text{CN})_x(\text{PMe}_3)_2]\}^+[\text{PF}_6]^-$, one of which has been isolated and characterized. The loss of activity in acetonitrile is attributed to the good ligating ability of acetonitrile which blocks the coordination of D_2 to Fe^{II} , as well as to the rapid decomposition of the hydride in photolyzed CH_3CN solution. Less decomposition is observed in acetone, and H/D exchange activity is retained.

(3) Added Ligands. In the presence of CO, the H/D exchange reaction was very slow, indicating that CO is an inhibitor of this reaction by competing for the same coordination site as D_2 . Whereas added PMe_3 might also compete for the photoinduced open site, it can also act as a base, deprotonate the bridging hydride, and generate the inactive neutral binuclear compounds, which was the observation. In the presence of 5 equiv of PMe_3 , H/D exchange activity completely ceased within 4 h. Added alkenes also

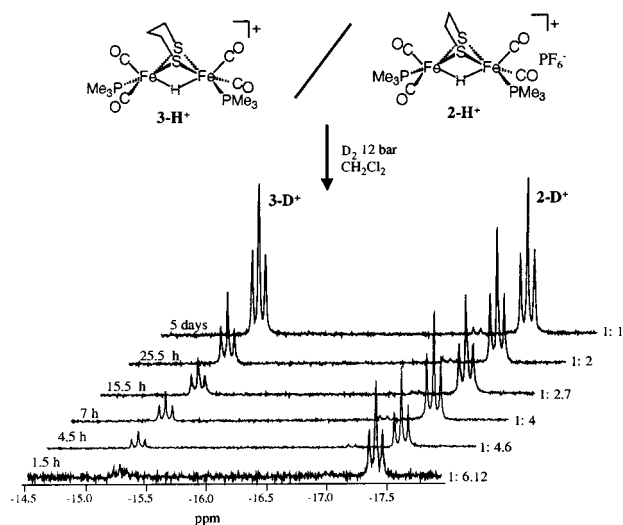


Figure 9. High field ²H NMR spectra of 1:1 mixture of **2-H⁺** and **3-H⁺** under 12 bar D₂ in CH₂Cl₂ solution at different sunlight exposure times.

impeded the build up of (*μ*-D)Fe₂⁺ species by blocking sites needed for D₂ binding.

(4) Counterion Effect. When the better coordinating anion [SO₃CF₃]⁻ was used as a counterion for **3-H⁺**, the solution changed color from red-orange to red-brown as H/D exchange occurred. The ²H NMR spectrum showed the high field *μ*-D resonance at -15.3 ppm as well as another hydride species as a doublet of doublets centered at -6.83 ppm with coupling constants of 3.50 and 4.72 Hz. Smaller counterions such as chloride promoted the deprotonation reactivity and decreased H/D exchange.

All of the described observations are consistent with the requirement of an open site for D₂ or H₂ binding prior to H/D exchange.

Ranking of H/D Exchange Activity. The following competition experiments were used to establish the relative order of H/D exchange reactivity within the series of *n*-H⁺ compounds. Mixtures of the hydride salts dissolved in CH₂Cl₂ and placed in NMR tubes were pressurized with D₂ and photolyzed by exposure to sunlight. The growth of *μ*-D signals was monitored by ²H NMR spectroscopy. For example, as shown in Figure 9, a sample composed of a 1:1 mixture of **2-H⁺** and **3-H⁺** showed the resonance at -17.44 ppm for **2-D⁺** to be clearly visible in 1.5 h, with only a minor signal at -15.3 ppm for **3-D⁺**. In 4.5 h, both had gained intensity with the relative integrated intensities of **2-D⁺**/**3-D⁺** = 4.6. With longer time, the *μ*-D signals both increased in intensity and equalized, reaching 1:1 within 5 days. Similarly, complexes **1-H⁺** and **2-H⁺** were compared for exchange with D₂, indicating a slightly greater exchange rate for the monodentate thiolate, SET. At 1 h of photolysis time, the signal intensity of **1-D⁺** = 1.7× that of **2-D⁺**. A 1:1:1 mixture of **2-H⁺**, **3-H⁺**, and **4-H⁺** showed uptake of D₂ and H/D exchange in relative ratio of 7.5:3:1 after an irradiation time of 1.5 h. A 1:1 mixture of **4-H⁺** and **7-H⁺** showed that the ratio of **4-D⁺**/**7-D⁺** was 1.68 after exposure to sunlight for 1.5 h under D₂. A 1:1 mixture of **1-H⁺** and **7-H⁺** showed that the ratio of the integrated signals **1-D⁺**/**7-D⁺** was 7:1 after 30 min of exposure to sunlight. Following the same

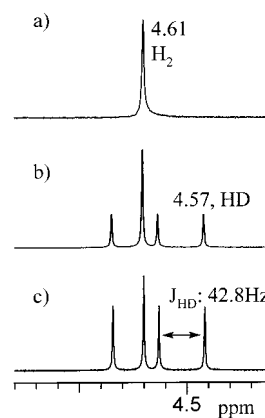


Figure 10. ¹H NMR spectra showing the relative ratio of HD/H₂ from a CD₂Cl₂ solution containing **3-H⁺**, 6 bar H₂, and 6 bar D₂: (a) before exposure to light; (b) 14 days exposure (1:1); (c) 40 days exposure (2:1).

procedure, the **5-H⁺** complex, containing PMe₂Ph ligands but otherwise structurally similar to **3-H⁺**, showed an H/D exchange capability comparable to that of the **3-H⁺** analogue. While these experiments established the relative order of H/D exchange, they also indicated inexact reproducibilities. Thus, while a numerical ranking is not allowed by our experimental design, the overall relative H/D exchange reactivity is given here. There is approximately an order of magnitude between the slowest and the fastest H/D exchange rates: **1-H⁺** > **2-H⁺** > **3-H⁺** > **4-H⁺** > **7-H⁺**.

Catalysis of HD Formation from H₂ and D₂. A medium-pressure NMR tube containing 10 mg (0.019 mmol) of **3-H⁺** in CD₂Cl₂ was pressurized with H₂ to 6 bar (0.60 mmol), followed by D₂ to 12 bar (0.60 mmol); the formation of HD was monitored by ¹H NMR. As shown in Figure 10a, the ¹H NMR spectrum taken before the sample was exposed to light only showed the presence of H₂ as a single peak at 4.6 ppm. After exposure to sunlight over the course of 2 days, a small triplet centered at 4.57 ppm with coupling constant of 42.8 Hz emerged, resulting from the formation of HD. The intensity of this triplet continued to increase with time, requiring under natural light conditions two weeks until its intensity became the same as that of H₂, Figure 10b. Full equilibration of H₂/HD/D₂ occurred over the course of several weeks, Figure 10c. This experiment clearly showed the catalytic ability of the hydride **3-H⁺**, as well as its stability in CH₂Cl₂. The upfield region of the sample showed that the hydride triplet at -15.3 ppm remained. When CH₂Cl₂ was used as solvent, the ²H NMR spectrum showed the catalytic formation of HD from H₂ and D₂ as a single peak at 4.67 ppm as well as the D₂ peak at 4.63 ppm.

H/D Exchange between D₂O and 3-H⁺. The ²H NMR spectrum of a CH₂Cl₂ solution of **3-H⁺** as its PF₆⁻ salt, containing 1–4 μL of D₂O, displayed signals at 1.67 ppm varying little with different amounts of D₂O. There was no formation of **3-D⁺**, even after standing for > 12 h in the dark. However, on exposure to sunlight for 5 h, the triplet at -15.3 ppm appeared in the ²H NMR spectrum, indicating H/D exchange with the bridging hydride. The intensity of this resonance was 0.27 relative to the solvent peak at 5.32 ppm, and the position of ¹H-enriched water shifted to 1.77 ppm. The intensity of the *μ*-D resonance peak increased slightly

after further exposure to sunlight. In comparison with the D_2 and $3-H^+$ reactivity, the H/D exchange in $3-H^+/D_2O$ was very slow. The latter exchange process was accelerated by the addition of PPN^+Cl^- , even in the absence of light.

$3-H^+$ Catalyzed H/D Exchange between H_2O and D_2 . Following standing in the dark for 12 h, a sample containing $3-H^+$, H_2O , and D_2 showed a resonance for dissolved D-enriched water at 1.63 ppm in the 2H NMR spectrum; its intensity was ca. 0.18 of the resonance for natural abundance deuterium in the CH_2Cl_2 solvent at 5.32 ppm. No signal was found for $3-D^+$ in the upfield region. When this sample was exposed to sunlight for 2 h, the characteristic triplet at -15.3 ppm in the 2H NMR indicated formation of $3-D^+$; its intensity was ca. 5.4 relative to the solvent peak. The resonance at 1.63 ppm shifted to 1.75 ppm and became very strong; its intensity was ca. 25 times that of the solvent peak. The other product, HD, appeared as a small peak at 4.67 ppm in the 2H NMR spectrum. Exposure to sunlight for 10 h resulted in no further changes in the dissolved water signal; however, the intensity of the bridging deuteride at -15.3 ppm increased to 7.6 times that of the solvent peak.

Extraneous Peaks. In our previous report¹⁸ and in the samples described here, a 2H NMR resonance found in the range 1.5–2.8 ppm for the H/D exchange reaction between $3-H^+$ and D_2 , and up to 10% of the $3-D^+$ resonance, was not assigned. This resonance varied its position in this range, differing from experiment to experiment; however, its intensity could not be correlated with the extent of H/D exchange into the bridging hydride position of the $n-H^+$. While the position of undissolved, or globules, of D_2O in CH_2Cl_2 is at 4.8 ppm, dissolved water in trace amounts is in the higher field region, ca. 1.70 ppm, and is the most reasonable candidate for this spurious peak. Thus, trace amounts of H_2O in the NMR tube while preparing the samples formed HDO or D_2O after the H/D exchange between H_2O and D_2 , catalyzed by $3-H^+$. So, the most reasonable candidate for the spurious peak is dissolved water. If not adventitious, dissolved water, present in the NMR tube, the “spurious peak” is a species that exchanges readily with D_2O . This was established by spiking samples with D_2O . There was no D incorporation to the methyl group of $[DP-(CH_3)_3]^+$, which, if so, would have appeared as a doublet at 1.89 ppm with coupling constant of 2.45 Hz. Control experiments showed that the position of $[DP(CD_3)_3]^+$ did not shift during the course of H/D exchange reaction.

The possibility that the spurious peak could be related to an S–D resonance remains, although SD derived from free $HS(CH_2)_3SH$ with 2H resonance at 1.42 ppm showed little position shift on addition of D_2O .

Stability of Hydrides in CH_2Cl_2 Solutions. Side by side stability comparisons of the PF_6^- salts of the hydrides $1-H^+$, $2-H^+$, $3-H^+$, $4-H^+$, and $5-H^+$, and $7-H^+$ as its $[SO_3CF_3]^-$ salt, in CH_2Cl_2 solutions were made in the same NMR tubes as used for H/D exchange studies. Pressurized with H_2 (7.5 bar) at room temperature and exposed to sunlight, these were sampled for IR spectra in the CO region. In all solutions, small amounts of an insoluble solid formed at the bottom of NMR tube, and the solution became darker compared with

the initial solution. The precipitate dissolved in acetone but showed no $\nu(CO)$ bands. After exposure to sunlight for 5 days, the IR monitor showed ca. 90% of $5-H^+$ remained in solution. Under the same conditions, ca. 84% of $3-H^+$ remained present in solution. Complex $2-H^+$ is less stable compared to $3-H^+$ and $5-H^+$; $2-H^+$ degraded by ca. 20% after only 3 days with exposure to sunlight. Compound $4-H^+$, which has $SCH_2C_6H_4CH_2S$ as bridging dithiolate, is the most unstable and decomposed completely in the same time period.

For compounds $1-H^+$ and $7-H^+$, there are isomerization processes which occur concomitantly with the decomposition process. Before irradiation, the IR spectrum of $1-H^+$ showed three CO bands at 2046(s), 2026(s), and 1991(s) cm^{-1} in CH_2Cl_2 solution. After exposure to sunlight for 5 days, the band pattern changed and shifted slightly to 2040(ms), 2026(s), and 1987(s) cm^{-1} ; a small band at 1867 cm^{-1} also appeared. The IR monitor showed ca. 70% of $1-H^+$ present in the solution. Under H/D exchange conditions, compound $7-H^+$ isomerized to $6-H^+$, the more stable isomer of the PS ligand derivative, over the course of 5 days. There was ca. 67% of the hydride remaining in solution. The order of the relative stability of all the hydrides studied is the following: $5-H^+ > 3-H^+ > 2-H^+ > 1-H^+ \approx 7-H^+ > 4-H^+$.

Conclusions

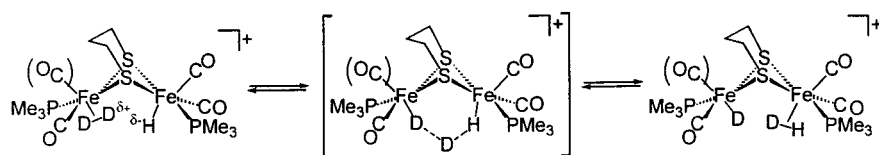
The H/D exchange processes that characterize H_2ase enzyme activity are observed in the dinuclear organometallic complexes $[Fe^II(\mu-H)Fe^II]^+$ of Chart 2, complexes which have structural features in common with the active site of $[Fe]-H_2ase$. The parent $(\mu-SRS)[Fe(CO)_3]_2$ reacts with added ligands such as CN^- or PR_3 to yield disubstituted complexes with complete regioselectivity in the product $(\mu-SRS)[Fe(CO)_2L]_2$. In contrast to their hexacarbonyl precursors, the Fe–Fe bonds of these complexes are sufficiently basic to be used in reactions with electrophiles (H^+ , SR^+). By this chemical reaction, the Fe centers achieve a +2 oxidation state wherein H_2 binding and heterolytic activation is facilitated. Thus, label scrambling in H_2/D_2 and H_2/D_2O mixtures requires protonation of the inactive Fe^I/Fe^I complexes, producing $[Fe^II(\mu-H)Fe^II]^+$ where two metals have shared the two-electron oxidative addition. It should be noted that such a chemical oxidation is not required to activate the binuclear enzyme active site for H_2 uptake as the redox activity of the enzyme permits electrochemical oxidation. However, the presence of a metal hydride is a mechanistic requirement for an H/D exchange activity pathway in H_2/D_2 mixtures.

While the remaining lone pair on sulfur of the bridging thiolate has been proposed as a repository for protons in theoretical model studies of hydrogenase activity of $[Fe]H_2ase$,⁴³ our results both in theory (the HOMO of the Fe^I/Fe^I complexes is the Fe–Fe bond density) and in experiment (the product of protonation is the $[Fe^II(\mu-H)Fe^II]^+$ complex) suggest otherwise.

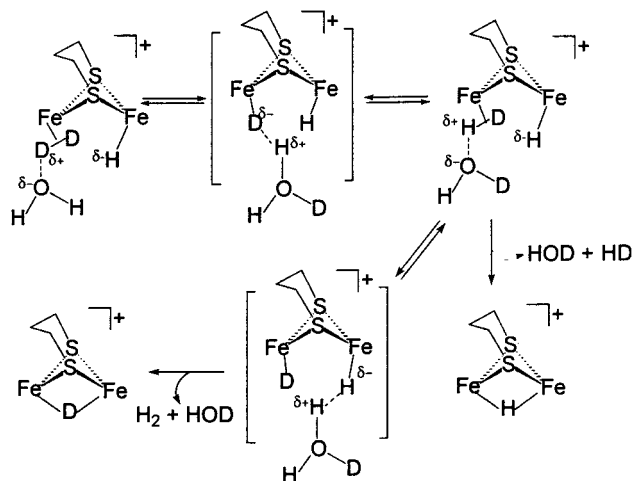
Both the H_2/D_2 and the H_2/D_2O exchange processes require photolysis, indicating the necessity for creating an open site

(43) (a) Cao, Z.; Hall, M. B. *J. Am. Chem. Soc.* **2001**, *123*, 3734. (b) Bruschi, M.; Fantucci, P.; De Gioia, L. *Inorg. Chem.* **2002**, *41*, 1421.

Scheme 1



Scheme 2



for H₂ or D₂ binding on the hydride-containing catalyst. As expressed earlier,¹⁸ this may result from CO loss or a hydride shift; if the former precedes η^2 -H₂ binding, a subsequent rotation and hydride shift (from bridging to terminal) is required for an internal heterolytic exchange process, Scheme 1. A stable form of such a species was reported for the complex (P-N)(η^2 -H₂)Ru(μ -Cl)₂(μ -H)Ru(H)(PPh₃)₂ (P-N = Fe(η -C₅H₃(CHMeNMe₂)P(i-Pr)₂-1,2)(η -C₅H₅)).⁴⁴ As shown in Scheme 1, positioning of the η^2 -H₂ in close proximity to the hydride gives opportunity for a trihydrogen transition state, formulated as a binuclear binding. The suggestion for such a species has precedence in the RuRu complex.⁴⁴ Nevertheless, a mononuclear trihydride or trihydrogen species located on a single metal is an alternate possibility, also with precedence.⁴⁵

Whereas H/D exchange into the μ -H position from D₂O is very slow, the presence of H₂ greatly accelerates the process. This exchange as well as the catalysis of H/D scrambling in an H₂/D₂O mixture is also explained on the basis of η^2 -H₂ binding to Fe^{II} and the greatly increased acidity resulting therefrom.⁴⁶ Scheme 2 displays a likely reaction scenario of events that follow, ultimately directing H/D exchange into the μ -H position.

In view of the promotional effect of water on the D₂/*n*-H⁺ H/D exchange process, one might question the validity of the intramolecular mechanism of Scheme 1. While the

effects of adventitious water would indeed be to promote such H/D exchange, numerous repetitions of the reactions under strenuously dry conditions yield the same results.

Relationships to the [Fe]H₂ase Enzyme Active Site. The minor structural differences between the neutral Fe^IFe^I and the protonated Fe^{II}(μ -H)Fe^{II} compounds suggest that the formation of such Fe^{II}Fe^{II} species could be a low activation barrier step in the catalytic mechanism of H⁺ uptake by the enzyme. Although the bridging thiolates have remarkable steric control of the position of substituent phosphines, there is no significant difference between the H/D exchange reactivities of the monodentate bridging thiolates and the bidentate analogues. From this, we conclude that the three light atom S to S linker cofactor is not required for at least some of the reactivity expected for the enzyme active site; two cysteines could have just as easily accomplished the bridging dithiolate structural features as indeed they do in the [NiFe]H₂ases.⁴⁷ Therefore, reasons for the presence of the pdt or μ -SCH₂NHCH₂S should lie in biosynthesis, active site import mechanisms, or the need to facilitate heterolytic H₂ activation by an internal amine base.³

The protonation of the Fe^I-Fe^I bond shifts the ν (CO) values ca. 80 cm⁻¹ higher than those of the neutral compounds and places them in the range of the as-isolated enzyme (1996 cm⁻¹).³ Only at the Fe^{II}Fe^{II} redox level do we see H/D exchange activity involving gaseous H₂ or D₂. We do not achieve mixed valent oxidation states in our studies. We do not see H₂ production from the [Fe^{II}(μ -H)-Fe^{II}]⁺ model complexes, as further protonation is impossible even with strong acids. Thus, H₂ formation must be preceded by reduction, at least to the Fe^{II}Fe^I, and possibly lower, redox states, as indicated by preliminary electrocatalytic generation of H₂ in our laboratories and others.⁴⁸ That H₂ uptake is at Fe^{II} centers is fully supported by our studies of the described homovalent, Fe^{II}Fe^{II} models.

Acknowledgment. We acknowledge financial support from the National Science Foundation (Grants CHE-9812355, CHE-0111629 for this work and CHE 85-13273 for the X-ray diffractometer and crystallographic computing system) and contributions from the R. A. Welch Foundation. Appreciation is expressed to Prof. Dieter Sellmann for encouraging this study. We would also like to thank Lisa Thomson for assistance with the computations and the Supercomputing Facility at Texas A&M University for

(44) (a) Hampton, C.; Cullen, W. R.; James, B. R. *J. Am. Chem. Soc.* **1988**, *110*, 6918. (b) Jackson, S. A.; Eisenstein, O. *Inorg. Chem.* **1990**, *29*, 3910.

(45) (a) Luo, X.-L.; Crabtree, R. H. *J. Am. Chem. Soc.* **1990**, *112*, 6912. (b) Maseras, F.; Lledós, A.; Clot, E.; Eisenstein, O. *Chem. Rev.* **2000**, *100*, 601.

(46) (a) Fong, T. P.; Lough, A. J.; Morris, R. H.; Mezzetti, A.; Rocchini, E.; Rigo, P. *J. Chem. Soc., Dalton Trans.* **1998**, 2111. (b) Abdur-Rashid, K.; Fong, T. P.; Greaves, B.; Gusev, D. G.; Himman, J. G.; Landau, S. E.; Lough, A. J.; Morris, R. H. *J. Am. Chem. Soc.* **2000**, *122*, 9155.

(47) (a) Volbeda, A.; Charon, M.-H.; Piras, C.; Hatchikian, E. C.; Frey, M.; Fontecilla-Camps, J. C. *Nature* **1995**, *373*, 580. (b) Volbeda, A.; Garcin, E.; Piras, C.; De Lacey, A. L.; Fernandez, V. M.; Hatchikian, E. C.; Frey, M.; Fontecilla-Camps, J. C. *J. Am. Chem. Soc.* **1996**, *118*, 12989. (c) Garcin, E.; Vernede, X.; Hatchikian, E. C.; Volbeda, A.; Frey, M.; Fontecilla-Camps, J. C. *Structure* **1999**, *7*, 557. (d) Higuchi, Y.; Yagi, T.; Yasuoka, N. *Structure* **1997**, *5*, 1671. (e) Higuchi, Y.; Ogata, H.; Miki, K.; Yasuoka, N.; Yagi, T. *Structure* **1999**, *7*, 549.

(48) Gloaguen, F.; Lawrence, J. D.; Rauchfuss, T. B. *J. Am. Chem. Soc.* **2001**, *123*, 9476.

computer time. R.M.-R. gratefully acknowledges the Universidad Autonoma de Queretaro and PROMEP for their support.

Supporting Information Available: Synthesis and characterization of compounds *n* and *n-H*⁺; molecular structure and X-ray

crystallographic tables for complexes **1**, **1-H**⁺, **2**, **2-H**⁺, **4**, **5-H**⁺; ¹³CO exchange experiments. This material is available free of charge via the Internet at <http://pubs.acs.org>.

IC020237R